HHS Public Access

Author manuscript

Biomacromolecules. Author manuscript; available in PMC 2023 January 10.

Published in final edited form as:

Biomacromolecules. 2022 October 10; 23(10): 4379–4387. doi:10.1021/acs.biomac.2c00831.

Cisplatin-Loaded Tobacco Mosaic Virus for Ovarian Cancer Treatment

Zhongchao Zhao,

Department of NanoEngineering, University of California, San Diego, La Jolla, California 92093, United States; Center for Nano-ImmunoEngineering, University of California, San Diego, La Jolla, California 92093, United States

Andrea Simms,

Department of NanoEngineering, University of California, San Diego, La Jolla, California 92093, United States

Nicole F. Steinmetz

Department of NanoEngineering, University of California, San Diego, La Jolla, California 92093, United States; Center for Nano-ImmunoEngineering, Department of Bioengineering, Department of Radiology, and Moores Cancer Center, University of California, San Diego, La Jolla, California 92093, United States; Institute for Materials Discovery and Design, University of California, La Jolla, California 92093, United States

Abstract

Ovarian cancer is the foremost cause of gynecological cancer and a major cause of cancer death in women. Treatment for advanced stage is surgical debulking followed by chemotherapy; however, most patients relapse with more aggressive and therapy-resistant tumors. There is a need to develop drug delivery approaches to deliver platinum therapies to tumors to increase efficacy while maintaining safety. Toward this goal, we utilized the protein nanotubes from the plant virus, tobacco mosaic virus (TMV), as a drug carrier. Specifically, the nanochannel of TMV was loaded with the active dication form of cisplatin ($cisPt^{2+}$), making use of the negatively charged Glu acid side chains that line the interior channel of TMV. We achieved a loading efficiency with ~2700 $cisPt^{2+}$ per TMV; formulation stability was established with drug complexes stably loaded into the carrier for 2 months under refrigerated storage. TMV-cisPt maintained its efficacy against ovarian tumor cells with an IC_{50} of ~40 μM. TMV-cisPt exhibited superior efficacy *vs* free cisPt in ovarian tumor mouse models using intraperitoneal ID8-Defb29/Vegf-a-Luc (mouse) tumors and subcutaneous A2780 (human) xenografts. TMV-cisPt treatment led to reduced tumor

Corresponding Author Nicole F. Steinmetz – Department of NanoEngineering, University of California, San Diego, La Jolla, California 92093, United States; Center for Nano-ImmunoEngineering, Department of Bioengineering, Department of Radiology, and Moores Cancer Center, University of California, San Diego, La Jolla, California 92093, United States; Institute for Materials Discovery and Design, University of California, La Jolla, California 92093, United States; nsteinmetz@ucsd.edu.

Supporting Information

The Supporting Information is available free of charge at https://pubs.acs.org/doi/10.1021/acs.biomac.2c00831.

TEM image of native TMV; individual tumor monitoring of circumference for the I.P.-treated mice; and individual tumor monitoring of tumor volume for the I.V.-treated mice (PDF)

The authors declare the following competing financial interest(s): Dr. Steinmetz is a co-founder of, has equity in and has a financial interest with Mosaic ImmunoEnginering Inc. Dr. Steinmetz serves as Director, Board Member, and Acting Chief Scientific Officer, and paid consultant to Mosaic. The other authors declare no potential COI.

burden and increased survival. Using ID8-Defb29/Vegf-a-Luc-bearing C57BL/6 mice, we also noted reduced tumor growth when animals were treated with TMV alone, which may indicate antitumor immunity induced by the immunomodulatory nature of the plant virus nanoparticle. Biodistribution studies supported the efficacy data, showing increased cisPt accumulation within tumors when delivered *via* the TMV carrier *vs* free cisPt administration. Finally, good safety profiles were noted. The study highlights the potential of TMV as a drug carrier against cancer and points to the opportunity to explore plant viruses as chemo-immuno combination cancer therapeutics.

Graphical Abstract

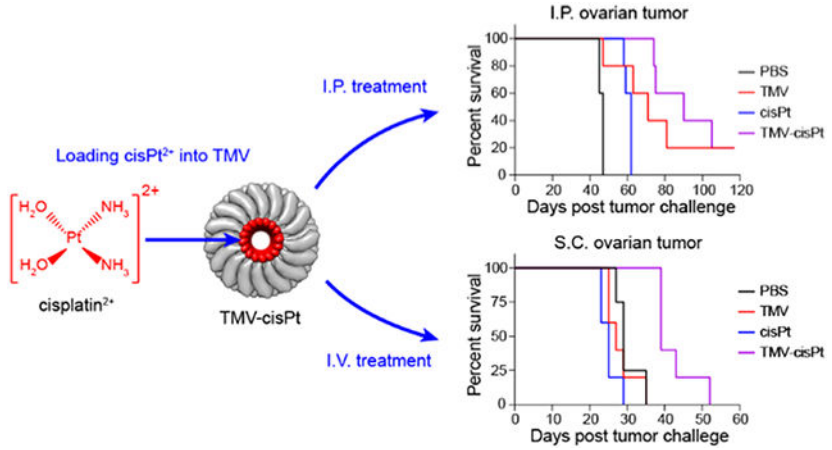

INTRODUCTION

Ovarian cancer is one of the deadliest gynecological cancers in women, and it is also the fifth most frequent cause of cancer death in women.[1,2] In 2022, it is estimated that 19880 women will be diagnosed with ovarian cancer and 12810 women will die from ovarian cancer in the United States.[1] Most cases are diagnosed at the advanced stage with metastatic disease; prognosis and survival rates are poor with a 5-year survival rate as low as ~30%.[3] Despite the recent advances and clinical trials with novel cancer therapies, surgical debulking and platinum-based chemotherapy are still the main strategies for ovarian cancer treatment. However, 80% of women with advanced-stage ovarian tumors will have tumor recurrence with drug resistance after surgical debulking and chemotherapy.[3] The challenge is reflected clearly in the “surgical debulking” terminology, *i.e.*, removing as much tumor as possible (along with the uterus and ovaries), but clearly not eliminating the disease.

Among the approved platinum drugs for ovarian cancer treatment, *cis*-diamminedichloridoplatinum(II) (cisplatin, cisPt) is one of the most commonly used and most effective drugs.[4] In fact, cisPt has been investigated in many clinical trials as a solo therapy or in combination.[5] Its mechanism of action is through the formation of DNA adducts leading to cancer cell apoptosis.[6] Despite its exceptional potency, free cisPt causes adverse effects, in particular nephrotoxicity, neurotoxicity, and myelosuppression.[7] More importantly, sub-optimal dosing can induce drug resistance. Platinum drug-resistant tumors

are a result of multiple mechanisms, including increased cisPt efflux, adapted DNA repair mechanisms, and cytosolic inactivation preventing DNA binding—cumulatively this leads to reduced active cisPt in cancer cells.[8-11] Drug delivery approaches could overcome these challenges because drug carriers have better safety profiles than free drugs and can enable tumor-specific accumulation. Here, we turned toward a plant virus nanoparticle platform technology for the delivery of cisPt.

Many different delivery systems have been developed for platinum-based drugs, including polymers, liposomes, gold nanoparticles, and virus-like particles, including plant viruses.[12-15] Each system has its advantages and disadvantages. Specifically, cisPt-loaded liposomes enhanced the circulation, but no efficacy improvement was observed due to the retention of cisPt within the liposomes;[16] cisPt conjugated to dendrimers and polymers increased the safety and reduced side effects, but often led to reduced efficacy;[17-19] cisPt conjugated to gold nanoparticles increased tumor killing efficacy with reduced side effects, but gold nanoparticles could cause organ damage due to high accumulation and slow clearance.[20] We chose the plant virus tobacco mosaic virus (TMV) as a drug carrier for the following reasons: TMV is proteinaceous and biodegradable; the unique shape of the nucleoprotein complex offers a 300 × 18 nm hollow nanotube that can accommodate cisPt and other chemotherapies in its 4 nm wide channel;[21,22] the high-aspect-ratio shape contributes to favorable biodistribution and tumor homing;[21,23] TMV can be produced with high yield through molecular farming in plants (15 mg/g infected leaf tissue);[24] and TMV does not infect mammals, therefore offering a higher degree of safety compared to mammalian viral vectors. TMV can be functionalized through drug encapsulation or surface conjugation. The TMV coat protein possesses surface-exposed tyrosine residues (one per coat protein, 2130 per TMV nanoparticle), which can be utilized to conjugate functional moieties through bioconjugation.[25] Additionally, TMV-Lys and TMV-Cys mutants have also been developed, offering surface-exposed lysine or cysteine residues for conjugation *via N*-hydroxysuccinimide (NHS) chemistry or maleimide chemistry.[26] In previous work, we demonstrated loading of TMV with phenanthriplatin[22] and mitoxantrone[27] achieving exceptional efficacy against tumors in mouse models. We also developed strategies for cisPt loading into TMV and confirmed the TMV-cisPt delivery to ovarian tumor cells *in vitro*, achieving efficacy even in ovarian tumor cells resistant to platinum therapy.[28] Building upon this work, in this study, we investigated the feasibility ofusing TMV as the delivery system for cisPt and the treatment efficacy of TMV-cisPt *in vivo* using two different ovarian tumor mouse models: an intraperitoneal (I.P.) ID8-Defb29/Vegf-a-Luc tumor model and a subcutaneous (S.C.) A2780 xenograft tumor model. Biodistribution and safety were also investigated.

MATERIALS AND METHODS

Production of TMV and TMV-cisPt.

TMV was propagated and purified from *Nicotiana benthamiana* plants,[24] and TMV-cisPt was prepared similarly to the previously published protocol.[28] In brief, cisPt and $AgNO_3$ were first dissolved in 50 mM HEPES, pH 7.5, then $cisPt^{2+}$ was obtained by mixing cisPt and $AgNO_3$ solutions with a 1:1.97 molar ratio overnight to precipitate AgCl.[29]

The next morning, AgCl was removed by two cycles of centrifugation at 14000*g* for 10 min; $cisPt^{2+}$ was recovered in the supernatant. TMV in 50 mM KP buffer, pH 7.4, was immediately added to the $cisPt^{2+}$ solution with a 20k molar excess ($cisPt^{2+}$ to TMV); TMV was maintained at a mixing concentration of 3.5 mg/mL. The mixture was incubated at room temperature for 2 h to achieve $cisPt^{2+}$ loading *via* electrostatic interactions into the negatively charged interior TMV channel. $cisPt^{2+}$-loaded TMV (referred to as TMV-cisPt) was purified over a 40% (w/v) sucrose cushion with ultracentrifugation at 160000*g* (Beckman Coulter) for 1 h at 4 °C. Free $cisPt^{2+}$ was removed using a two-step protocol: first, the TMV-cisPt pellet after sucrose cushion was rinsed twice using PBS (pH 7.4) and then resuspended in PBS; second, the resuspended TMV-cisPt solution was further purified over a PD-10 desalting column (Cytiva). The TMV concentration was determined by UV–vis spectrophotometry (NanoDrop 2000, Thermo Scientific) using the TMV-specific extinction coefficient TMV ε (260 nm) = 3 mL/(mg cm), and the $cisPt^{2+}$ concentration was determined using inductively coupled plasma mass spectrometry (ICP-MS). To prepare samples for ICP-MS, 1 μL of TMV-cisPt was mixed with 499 μL of concentrated nitric acid (Fisher Scientific) and 500 μL of Milli-Q water and heated for 10 min at 95 °C. Then, the 1 mL solution was further diluted to 10 mL using Milli-Q water prior to analysis by ICP-MS (iCAP RQ, Thermo Fisher). The structural integrity of TMV-cisPt was confirmed by transmission electron microscopy (TEM). TMV-cisPt (4 μL, 0.5 mg/mL) was applied to a glow-discharged carbon film with a 300-mesh Cu grid for 30 s, blotted using filter paper, and then stained with 4 μL of 0.75% (w/v) uranyl formate (UF) for 30 s, blotted again using filter paper. After one-time washing using 4 μL of Milli-Q water, the grid was blotted again using filter paper and air-dried. Images were collected using a Thermo Fisher Talos Transmission Electron Microscope at a nominal magnification of ×120000.

Cell Lines and Cell Culture.

The murine ovarian cancer cell line ID8-Defb29/Vegf-a-Luc[30] was cultured using RPMI 1640 [+] L-glutamine medium (Corning) supplemented with 10% (v/v) fetal-bovine serum (FBS) (VWR), 1% (v/v) penicillin/streptomycin (Pen/Strep) (Cytiva), 1 mM sodium pyruvate (Thermo Fisher Scientific), and 0.05 mM 2-mercaptoethanol (Thermo Fisher Scientific). Human ovarian cancer cell line A2780 (ATCC) was cultured using RPMI 1640 [+] L-glutamine medium (Corning) supplemented with 10% (v/v) FBS (VWR), and 1% (v/v) Pen/Strep (Cytiva). Both cell lines were maintained at 37 °C with 5% CO_2.

Cytotoxicity Assay.

The cytotoxicity of the cisPt *vs* TMV-cisPt against ID8-Defb29/Vegf-a-Luc and A2780 cells was determined using the 3-(4,5-dimethylthiazol-2-yl)-2,5-diphenyltetrazolium bromide (MTT) assay kit (Abcam). Each assay was performed in triplicate using 96-well plates; PBS and TMV served as negative controls. 5×10^3 ID8-Defb29/Vegf-a-Luc cells in 100 μL of media and 10×10^3 A2780 cells in 100 μL of media were plated in each well and incubated for 24 h prior to treatment. After removing media, the cells were treated with TMV-cisPt or cisPt in the range of 0.01–500 μM cisPt; PBS and TMV were used as negative controls. The concentration of TMV was normalized to the TMV-cisPt concentration; treatment was for 24 h at 37 °C with 5% CO_2. As per the manufacturer's recommendation, the media was then removed and MTT reagent plus serum-free media were added into each well for

3 h incubation at 37 °C with 5% CO_2. Finally, MTT reagent and media were removed and MTT solvent was added into each well for 15 min with orbital shaking. Absorbance readings at 570 nm were recorded using a Tecan plate reader, and cell viability and inhibitory concentration 50% (IC_{50}) were calculated based on the readings.

Mice.

All mouse studies were carried out in accordance with the guidelines of the Institutional Animal Care and Use Committee (IACUC) of the University of California, San Diego (UCSD) and were approved by the Animal Ethics Committee of UCSD. All experiments were conducted using 6- to 8-week-old mice. Female C57BL/6 mice were purchased from Jackson Laboratories for I.P. ID8-Defb29/Vegf-a-Luc tumor studies, and female NCR nu/nu mice were purchased from the In-House Breeding Colony of UCSD for S.C. A2780 xenograft tumor studies. Only female mice were used because ovarian cancer only afflicts women.

Tumor Inoculations and Treatments.

For the I.P. ID8-Defb29/Vegf-a-Luc tumor inoculations, cells were harvested and washed once using PBS and resuspended in PBS giving 10×10^6 cells per mL, then 2×10^6 cells in 200 μL were I.P. injected into each mouse on day 0. I.P. tumor burden was monitored three times per week by measuring mice body weights and circumferences. Seven days post tumor inoculation, four groups of mice ($n = 5$) were treated I.P. with 200 μL of PBS, 200 μL of 5 mg/mL TMV, 200 μL of 0.1 μg/μL cisPt, and 200 μL of 0.1 μg/μL TMV-cisPt (cisPt concentration is listed); this equates to a dose of 20 μg cisPt per mouse or ~1 mg cisPt/kg body weight. All mice were treated twice per week for 6 weeks. The mice were euthanized when their body weight reached 35 g or circumference reached 9 cm. A2780 tumors were inoculated S.C. using female NCR nu/nu mice; the cells were harvested and resuspended in culture media with 40×10^6 cells/mL and then mixed with Matrigel (Corning) at a 1:1 ratio. The mixed A2780 cells (2×10^6) in 100 μL were S.C. injected into the right flank of each mouse on day 0. Tumor growth was monitored closely by measuring the tumor volume. When tumors reached 200–300 mm^3 on day 7, four groups of mice ($n = 5$) were treated with 100 μL of PBS, 100 μL of 10 mg/mL TMV, 100 μL of 0.2 μg/μL cisPt, and 100 μL of 0.2 μg/μL TMV-cisPt (cisPt concentration is listed) through intravenous (I.V.) injection. All of the mice were treated every 2 days until the endpoint was reached. The mice were euthanized when their tumor volumes reached 1500 mm^3. Tumor volume was calculated using the formula $v = l \times \frac{w^2}{2}$, where l is the length of the tumor and w is the width.

Biodistribution.

Tumor challenge was performed as described above. For the ID8-Defb29/Vegf-a-Luc I.P. tumor model, 2×10^6 cells in 200 μL were I.P. injected into each mouse on day 0. 40 days post tumor inoculation, the mice were I.P. -treated with 200 μL of PBS, 200 μL of 0.1 μg/μL cisPt, or 200 μL of 0.1 μg/μL TMV-cisPt (cisPt concentration is listed) (5 mice per group). For the A2780 S.C. tumor model, 2×10^6 of A2780 cells mixed with Matrigel in 100 μL were S.C. injected into the right flank of each mouse on day 0. Eleven days post tumor inoculation, the mice were I.V. treated with 100 μL of 0.2 μg/μL TMV-cisPt

(cisPt concentration is listed), 100 μL of 0.2 μg/μL cisPt, and 100 μL of PBS (7 mice per group). 24 h post treatment injections for both tumor models, the mice were sacrificed and organs (brain, heart, lung, kidney, spleen, and liver) and tumors were collected for cisPt quantification using ICP-MS. To prepare samples for ICP-MS analysis, tissues were weighed and digested in 500 μL of concentrated nitric acid (Fisher Scientific) by heating at 95 °C for 20 min to dissolve all tissues. Milli-Q water (4.5 mL) was added into each sample to dilute the concentrated nitric acid. Leftover tissue debris was removed by centrifuging at 15000*g* for 7 min, and the supernatants were analyzed on ICP-MS. Four concentrations of ICP-MS platinum standards were prepared using the Platinum Standard for ICP (Sigma-Aldrich).

Organ Toxicity.

Alanine Transaminase (ALT), Aspartate Aminotransferase (AST), and Kidney Injury Molecule 1 (KIM-1) assays were performed to assess organ toxicity. After the I.P. ID8-Defb/Vegf-a-Luc tumor inoculation on day 0, C57BL/6 mice ($n = 5$) were treated three times on days 7,10, and 14 *via* I.P. injection with cisPt or TMV-cisPt (20 μg cisPt per mouse or ~1 mg cisPt/kg body weight for injection); PBS and TMV were injected as negative controls. The TMV dose was normalized to match the TMV-cisPt dose. One and five days after the third injection, blood was collected through retro-orbital bleeding using heparinized tubes (Fisher Scientific). The blood was centrifuged at 5283*g* for 10 min at 4 °C, and the plasma was collected and stored at −80 °C. Following the assay protocols, we used an Alanine Transaminase Activity Assay Kit, Aspartate Aminotransferase Activity Assay Kit, and Mouse KIM-1 ELISA Kit from Abcam to test the ALT, AST, and KIM-1 of the plasma. Briefly, the plasma was diluted 10 times using the corresponding assay buffer and the ALT activity, AST activity, and KIM-1 content were assayed and calculated based on the standard curves. Absorbance readings at 570 nm at 50 and 60 min were used to calculate the ALT activity, absorbance readings at 450 nm at 50 and 60 min were used to calculate the AST activity, and absorbance readings at 450 nm were used to calculate the KIM-1 content using a Tecan plate reader.

RESULTS AND DISCUSSION

Synthesis and Characterization of TMV-cisPt.

TMV was purified from *N. benthamiana* plants.[24] Each TMV consists of 2130 copies of identical TMV coat protein (CP) units arranged into a hollow nanotube with a 4 nm wide channel[31] (Figure 1A). Each CP has two glutamic acids, Glu 97 and Glu 106, located inside the nanochannel, giving a negatively charged interior with 4260 glutamic acids. The Glu residues can be deprotonated to coordinate and load positively charged therapeutic molecules through electrostatic interactions.[27-29,32] Here, we utilized established protocols to load $cisPt^{2+}$ into TMV.[28] To achieve efficient TMV encapsulation, charged $cisPt^{2+}$ was generated by mixing noncharged cisPt with $AgNO_3$ in solution to remove the two Cl^- ions from cisPt[29] (Figure 1B); Ag^+ reacts with Cl^- to form a precipitate, leaving $cisPt^{2+}$ in solution. The $cisPt^{2+}$ cation was then mixed with TMV at pH 7.4 to yield TMV-cisPt. TMV-cisPt was purified through ultracentrifugation and gel filtration to remove excess $cisPt^{2+}$, leading to pure TMV-cisPt. The loading efficiency of $cisPt^{2+}$ was determined

using the molar ratio of cisPt to TMV (mol cisPt:mol TMV), where the Pt concentration was measured using ICP-MS and the TMV concentration was measured using UV–vis spectroscopy. To test the stability of purified TMV-cisPt at 4 °C for storage, the $cisPt^{2+}$ concentration was tested using ICP-MS for about 2 months. Prior to each measurement, we performed buffer exchange to remove any $cisPt^{2+}$ that may have leached from the TMV carrier through its open ends. We observed an initial drop of $cisPt^{2+}$ concentration from ~3500 cisPt per TMV on day 0 to ~2800 cisPt per TMV on day 2, which may be due to the loss of less-stably bound $cisPt^{2+}$ during the gel filtration step as part of ICP-MS sample preparation after day 0. However, the $cisPt^{2+}$ concentration then remained consistent at ~2700 cisPt per TMV throughout the 2-month span (Figure 1C), which indicates good stability and shelf-life of the TMV-cisPt complex. Using transmission electron microscopy (TEM) (Figure 1D), we confirmed structural integrity and observed the rod-shaped structure of TMV-cisPt was similar to wild-type TMV (Figure S1), indicating the loading process did not alter the structure of TMV. It is of note that in the present study, we observed relatively higher loading efficiency with 2500–3000 cisPt per TMV, compared to what we previously reported, *i.e.*, ~2000 cisPt per TMV. This may be explained by differences in the protocols, as in the present study higher cisPt/TMV loading concentrations were used. Data may indicate that maximum loading capacity is achieved given each TMV particle offers 4260 Glu acids. This means that there are 4260 negative charges to complex 2130 $cisPt^{2+}$ molecules.

Free cisPt is required to undergo hydrolysis and removal of the two Cl^- ions prior to binding to DNA to form DNA adducts and exert its toxicity.[33] Unionized cisPt is the dominant form in blood because blood has high Cl anion concentrations (105 mM Cl^- ions), which suppresses the formation of the cationic $cisPt^{2+}$ form.[34] While this confers safety, free cisPt can also be captured by blood plasma proteins, especially human serum albumin.[35] Soluble cisPt therefore may not confer the most potent efficacy. Our TMV-cisPt formulation may resolve these issues through “preactivation” of cisPt into its active $cisPt^{2+}$ form and packaging and stabilizing $cisPt^{2+}$ within TMV’s nanochannel, which not only increases its potency through delivery of the active form to cancer cells but also protects it from interaction with serum proteins.[36]

TMV-cisPt Cytotoxicity.

To test the cancer-killing ability of TMV-cisPt, we performed MTT assays by treating two ovarian cancer cell lines, ID8-Defb29/Vegf-a-Luc cells (mouse-derived) and A2780 cells (human-derived) with cisPt and TMV-cisPt; PBS and TMV were used as negative controls. Data indicate potent and matched efficacy of TMV-cisPt *vs* cisPt for both cell lines. As expected, there was no efficacy of the empty carrier: TMV-treated cells matched the PBS group, and there were no signs of toxicity from TMV (Figure 2A,B). We determined the IC_{50} and found that TMV-cisPt and cisPt have a similar IC_{50} in the range of 30–50 μM, independent of both tested cell lines (Figure 2C). We note that in previous studies, we observed improved efficacy of TMV-cisPt *vs* free cisPt in tissue culture experiments,[28] which may be due to differences in cell seeding and incubation times. Such changes could affect the overall cell killing. Nevertheless, overall these data are in good agreement with the literature and other reported cisPt nanocarrier systems.[38,39]

TMV-cisPt Efficacy against Ovarian Tumors *In Vivo*.

Previous biodistribution and imaging studies indicate good tumor homing properties of TMV;[21,22] therefore, we went on to assess the efficacy of TMV-cisPt *in vivo*. To evaluate the *in vivo* efficacy of TMV-cisPt for cancer treatment, we used two different ovarian tumor mouse models: an ID8-Defb29/Vegf-a-Luc tumor model using C57BL/6 mice where tumors are established as a disseminated metastatic disease in the I.P. space, and an S.C. A2780 xenograft model using NCR nu/nu mice—the latter allows testing against cells derived from human ovarian tumors. The I.P. tumor model closely resembles the human ovarian cancer with metastasis occurring in the peritoneal cavity. The peritoneal cavity is isolated by the peritoneal wall; direct I.P. treatment is somewhat localized and increases tumor interactions of therapeutics (here as for TMV-cisPt) within the I.P. cavity, which can increase efficacy and decrease the off-target side effects observed by I.V. injections.[40] I.P. administration of therapeutics is also feasible in patients with ovarian tumors.[41] For the I.P. ID8-Defb29/Vegf-a-Luc tumor model, we inoculated 2×10^6 cells and started I.P. treatments 7 days post tumor challenge for 6 weeks with two injections per week of TMV-cisPt, free cisPt, and two controls PBS and TMV in 200 μL (Figure 3A). The injection dose of TMV-cisPt and free cisPt was 20 μg cisPt per mouse or 1 mg/kg (cisPt/mouse) as established in our previous studies;[15,22] the dose of free TMV (~1 mg) was normalized to TMV-cisPt. Tumor progression was monitored using the increase in body weight and circumference resulting from tumor burden and ascites development (Figure 3B,C). The mice were euthanized when the endpoint, defined as 35 g body weight or 9 cm circumference, was reached. Untreated mice (PBS group) showed a steep rise of body weight and circumference 35 days post tumor inoculation. cisPt treatment only marginally delayed the tumor onset until 49 days, but this was followed by aggressive tumor progression. Somewhat surprisingly for the TMV-treated group, other than one mouse that died on day 47 due to high tumor burden, the remainder of the group showed slower tumor progression than both the PBS control and cisPt treatment groups. In stark contrast, TMV-cisPt significantly delayed the tumor growth in all mice with no signs of tumor growth until day 63 (Figure 3B, see also Figure S2). These results were also reflected in the survival curves (Figure 3D). The TMV-cisPt group had a median survival of 90 days, with two mice surviving for longer than 100 days, while the cisPt group with 62 days, the TMV group with 71 days, and the PBS group with 47 days. These data consistently show improved efficacy of TMV-cisPt *vs* free cisPt in this ovarian tumor mouse model.

Next, efficacy was tested using the A2780 xenografts tumor model with S.C. tumor challenge using 2×10^6 cells in Matrigel. Treatment began on day 7 post tumor challenge, when tumors reached 200–300 mm^3—here, the animals were treated I.V. every 2 days using the same dosage as reported above but with an injection volume of 100 μL (Figure 3E). Tumor burden was monitored by measuring the increase of the tumor volumes (Figure 3F). Body weight was also monitored as an indication of adverse effects (Figure 3G), but our measurements demonstrated no loss of body weight, thus contributing a sign of the safety of our formulations. The mice were euthanized when tumor volumes reached 1500 mm^3. TMV-cisPt treatment significantly slowed tumor growth, indicating the successful delivery of $cisPt^{2+}$ to tumors by TMV-cisPt (Figure S3). Potent efficacy of TMV-cisPt was also

reflected by the survival curves (Figure 3H). The TMV-cisPt-treated mice had a median survival of 39 days, while all other groups had a median survival below 29 days.

Overall data in the two mouse models consistently illustrate potency of the TMV-cisPt delivery system. However, one difference was apparent: while TMV slowed tumor growth in the ID8-Defb29/Vegf-a-Luc model in the C57BL/6 mice, this effect was not apparent in the A2780 model using immunodeficient NCR nu/nu nude mice. We have previously observed that plant viruses without payload can induce antitumor responses after *in situ* or systemic administration,[42-45] and this is explained by their immunomodulatory nature. Noninfectious plant viruses are recognized as foreign materials and activate innate immunity, which can stimulate antitumor immune responses. This of course is more profound in the C57BL/6 mice because, while the immunocompromised nude mice still have components of the innate immune system, they lack adaptive immunity.[15,22,27] The immunomodulatory nature of the carrier system thus may add to the therapeutic efficacy of TMV-cisPt.

TMV-cisPt Biodistribution.

To validate that the improved tumor treatment efficacy of TMV-cisPt was indeed based on increased drug delivery to the tumor, we conducted biodistribution studies in both tumor models. For the ID8-Defb29/Vegf-a-Luc tumor model in C57BL/6 mice, we inoculated tumors I.P. using 2×10^6 cells on day 0. Biodistribution was studied on day 40, and tumor burden was apparent by increase in circumference. On day 40, 20 μg of TMV-cisPt or free cisPt in 200 μL of PBS was administered I.P.; 200 μL of PBS was injected as a negative control. 24 hours post injections, organs and tumors were harvested (Figure 4A). For the S.C A2780 tumor model in NCR nu/nu nude mice, we inoculated tumors S.C. using 2×10^6 cells; at 11 days post-challenge when tumors reached over 300 mm^3, 20 μg of TMV-cisPt or free cisPt in 100 μL of PBS, with 100 μL of PBS as a negative control, were I.V. injected. And 24 h post injection, organs and tumors were harvested (Figure 4D). All organs and tumors were processed for ICP-MS to determine the cisPt content in organs and tumors (normalized to weight).

We observed a higher platinum content in all organs and the tumors of the TMV-cisPt group compared to the free cisPt group (Figure 4B,E). The cisPt content was significantly increased in tumors of the TMV-cisPt group compared to the free cisPt group. For the I.P. ID8-Defb29/Vegf-a-Luc tumor model, ~0.45 μg of cisPt was accumulated in 1 g of tumor tissues, compared to ~0.09 μg cisPt per g tumor for the free cisPt group—a 5-fold increase. The S.C. A2780 xenograft tumor model showed a similar trend, albeit with a lower increase: ~0.11 μg of cisPt per g tumor tissue for the TMV-cisPt *vs* ~0.07 μg of cisPt per g tumor for the free cisPt group. Greater tumor accumulation can be explained by the passive targeting of TMV nanoparticles to tumor based on the enhanced permeability and retention (EPR) effect.[15,32,46]

More cisPt from the TMV-cisPt formulation was observed in the liver and spleen, which agrees with our previous result[47] that clearance of the TMV is mainly through the mononuclear phagocyte system (liver and spleen). TMV has a 300 nm × 18 nm size, which fits in the 10–200 nm range for both liver and spleen clearance.[48] Significant amounts of cisPt from the TMV-cisPt treatment were also observed in the kidneys, indicating that

TMV-cisPt was also cleared through the renal system. Although TMV is over the size limit (15 nm) for renal filtration,[48] different studies have shown that nanotube structures including carbon nanotubes (CNT)[49] and potato virus X (PVX)[50] may align in the glomerular filtration and therefore pass through the kidneys. Finally, we observed the elongated nanotube structure could also lead to accumulation in the lungs.[51,52] The accumulation in the lungs will require further investigation. Lung accumulation may be a result of protein corona formation and/or aggregation, which may be mitigated through appropriate surface coatings, such as PEGylation. While organ accumulation of TMV-cisPt was apparent, we did not observe a loss of body weight, a measure of toxicity (see Figure 3C,G).

TMV-cisPt Toxicology.

Although toxicity was not apparent based on body weight measurements (see Figure 3C,G), we further examined potential liver and kidney damages and compared TMV-cisPt *vs* free cisPt. Because both ID8-Defb29/Vegf-a-Luc tumor model and S.C. A2780 tumor model showed a similar biodistribution pattern, we chose the nonimmunocompromised ID8-Defb29/Vegf-a-Luc-bearing C57BL/6 mice for this study. Similar to the treatment schedule (Figure 3A), 7 days after the tumor inoculation, the mice received three doses of 20 μg of TMV-cisPt and free cisPt in 200 μL of PBS I.P.; 1 mg of TMV in 200 μL of PBS and pure PBS were administered as controls (Figure 5A). One day and five days after the third injection, blood was collected by retro-orbital bleeding and plasma was prepared for ALT, AST, and KIM-1 assays. Both ALT and AST are indicators of liver damage, and KIM-1 is an indicator of kidney damage. For the ALT assay, ALT activities in all treated mice were in the normal range[53] of healthy mice on day 1 and day 5 following the third injection (Figure 5B). TMV-cisPt-treated mice showed higher levels of AST activity on day 1; however, this then fell back into the normal range by day 5 (Figure 5C). Hence, data may indicate potential liver toxicity because chemotherapy regimens are often given repeatedly over extended time periods; this will require further follow-up investigation. Importantly, KIM-1 levels were found to be in the normal range[54] independent of treatment, indicating that the dose range was safe and there was no evidence of kidney injury (Figure 5D).

CONCLUSIONS

We formulated TMV-cisPt by loading $cisPt^{2+}$ into the nanochannel of TMV and achieved drug delivery and treatment of ovarian cancer in both *in vitro* and *in vivo* models. TMV-cisPt maintained its cytotoxicity against ovarian cancer cells. Using two mouse models, an orthotopic mouse tumor model and human xenograft model, we confirmed *in vivo* efficacy of TMV-cisPt. TMV-cisPt demonstrated increased potency against ovarian tumors compared to free cisPt, which was evident by reduced tumor burden and increased survival. Biodistribution corroborated the data and indicated increased cisPt delivery by TMV with enhanced tumor accumulation. In addition to conferring efficacy as a drug delivery vehicle, the immunostimulatory nature of TMV also provided efficacy and reduced tumor growth. Therefore, this study also highlights the opportunity to explore immuno-chemo combination therapies making use of TMV or other plant viral nanocarriers. In summary, our data further validated the TMV-cisPt platform for ovarian cancer therapy. Of course, the principles

explored could also be adapted to the delivery of other small-molecule drugs targeting various tumor types.

Supplementary Material

Refer to Web version on PubMed Central for supplementary material.

ACKNOWLEDGMENTS

This work was supported in part by the NIH (R01-CA253615 and R01 CA224605) and the Shaughnessy Family Fund for Nano-ImmunoEngineering (nanoIE) at UCSD.

REFERENCES

(1). Board, P. A. T. E. Ovarian Epithelial, Fallopian Tube, and Primary Peritoneal Cancer Treatment (PDQ). https://www.cancer.gov/types/ovarian/hp/ovarian-epithelial-treatment-pdq; National Cancer Institute (US) (accessed June 01, 2022).

(2). Arora T; Mullangi S; Lekkala MR Ovarian cancer. In StatPearls. https://www.ncbi.nlm.nih.gov/books/NBK567760/ (accessed June 01, 2022).

(3). Siegel RL; Miller KD; Jemal A Cancer statistics, 2020. Ca-Cancer J. Clin 2020, 70, 7–30. [PubMed: 31912902]

(4). Ghosh S Cisplatin: The first metal based anticancer drug. Bioorg. Chem 2019, 88, No. 102925. [PubMed: 31003078]

(5). Kopacz-Bednarska A; Król T Cisplatin—properties and clinical application. Oncol. Clin. Pract 2022, 18, 166–176.

(6). Tanida S; Mizoshita T; Ozeki K; Tsukamoto H; Kamiya T; Kataoka H; Sakamuro D; Joh T Mechanisms of cisplatin-induced apoptosis and of cisplatin sensitivity: potential of BIN1 to act as a potent predictor of cisplatin sensitivity in gastric cancer treatment. Int. J. Surg. Oncol 2012, 2012, No. 862879. [PubMed: 22778941]

(7). Duan X; He C; Kron SJ; Lin W Nanoparticle formulations of cisplatin for cancer therapy. Wiley Interdiscip. Rev.: Nanomed. Nanobiotechnol 2016, 8, 776–791. [PubMed: 26848041]

(8). Galluzzi L; Senovilla L; Vitale I; Michels J; Martins I; Kepp O; Castedo M; Kroemer G Molecular mechanisms of cisplatin resistance. Oncogene 2012, 31, 1869–1883. [PubMed: 21892204]

(9). Moitra K; Lou H; Dean M Multidrug efflux pumps and cancer stem cells: insights into multidrug resistance and therapeutic development. Clin. Pharmacol. Ther 2011, 89, 491–502. [PubMed: 21368752]

(10). Fletcher JI; Haber M; Henderson MJ; Norris MD ABC transporters in cancer: more than just drug efflux pumps. Nat. Rev. Cancer 2010, 10, 147–156. [PubMed: 20075923]

(11). Cho K; Wang X; Nie S; Chen ZG; Shin DM Therapeutic nanoparticles for drug delivery in cancer. Clin. Cancer Res 2008, 14, 1310–1316. [PubMed: 18316549]

(12). Wang B; Wang S; Zhang Q; Deng Y; Li X; Peng L; Zuo X; Piao M; Kuang X; Sheng S; Yu Y Recent advances in polymer-based drug delivery systems for local anesthetics. Acta Biomater. 2019, 96, 55–67. [PubMed: 31152941]

(13). Naguib YW; Rodriguez BL; Li X; Hursting SD; Williams RO III; Cui Z Solid lipid nanoparticle formulations of docetaxel prepared with high melting point triglycerides: in vitro and in vivo evaluation. Mol. Pharmaceutics 2014, 11, 1239–1249.

(14). Mukerabigwi JF; Ge Z; Kataoka K Therapeutic nanoreactors as in vivo nanoplatforms for cancer therapy. Chem. - Eur. J 2018, 24, 15706–15724. [PubMed: 29572992]

(15). Hu H; Steinmetz NF Cisplatin Prodrug-Loaded Nanoparticles Based on Physalis Mottle Virus for Cancer Therapy. Mol. Pharmaceutics 2020, 17, 4629–4636.

(16). White SC; Lorigan P; Margison GP; Margison JM; Martin F; Thatcher N; Anderson H; Ranson M Phase II study of SPI-77 (sterically stabilised liposomal cisplatin) in advanced non-small-cell lung cancer. Br J Cancer 2006, 95, 822–828. [PubMed: 16969346]

(17). Fujiyama J; Nakase Y; Osaki K; Sakakura C; Yamagishi H; Hagiwara A Cisplatin incorporated in microspheres: development and fundamental studies for its clinical application. J Controlled Release 2003, 89, 397–408.

(18). Haxton KJ; Burt HM Polymeric drug delivery of platinum-based anticancer agents. J. Pharm. Sci 2009, 98, 2299–2316. [PubMed: 19009590]

(19). Lin X; Zhang Q; Rice J; Stewart D; Nowotnik D; Howell S Improved targeting of platinum chemotherapeutics: the antitumour activity of the HPMA copolymer platinum agent AP5280 in murine tumour models. Eur. J. Cancer 2004, 40, 291–297. [PubMed: 14728945]

(20). Balasubramanian SK; Jittiwat J; Manikandan J; Ong C-N; Liya EY; Ong W-Y Biodistribution of gold nanoparticles and gene expression changes in the liver and spleen after intravenous administration in rats. Biomaterials 2010, 31, 2034–2042. [PubMed: 20044133]

(21). Shukla S; Eber FJ; Nagarajan AS; DiFranco NA; Schmidt N; Wen AM; Eiben S; Twyman RM; Wege C; Steinmetz NF The Impact of Aspect Ratio on the Biodistribution and Tumor Homing of Rigid Soft-Matter Nanorods. Adv. Healthcare Mater 2015, 4, 874–882.

(22). Czapar AE; Zheng YR; Riddell IA; Shukla S; Awuah SG; Lippard SJ; Steinmetz NF Tobacco Mosaic Virus Delivery of Phenanthriplatin for Cancer therapy. ACS Nano 2016, 10, 4119–4126. [PubMed: 26982250]

(23). Lee KL; Carpenter BL; Wen AM; Ghiladi RA; Steinmetz NF High Aspect Ratio Nanotubes Formed by Tobacco Mosaic Virus for Delivery of Photodynamic Agents Targeting Melanoma. ACS Biomater. Sci. Eng 2016, 2, 838–844. [PubMed: 28713855]

(24). Bruckman MA; Steinmetz NFChemical Modification of the Inner and Outer Surfaces of Tobacco Mosaic Virus (TMV). In Methods in Molecular Biology; Springer, 2014; Vol. 1108, pp 173–185. [PubMed: 24243249]

(25). Schlick TL; Ding Z; Kovacs EW; Francis MB Dual-surface modification of the tobacco mosaic virus. J. Am. Chem. Soc 2005, 127, 3718–3723. [PubMed: 15771505]

(26). Geiger FC; Eber FJ; Eiben S; Mueller A; Jeske H; Spatz JP; Wege C TMV nanorods with programmed longitudinal domains of differently addressable coat proteins. Nanoscale 2013, 5, 3808–3816. [PubMed: 23519401]

(27). Lin RD; Steinmetz NF Tobacco mosaic virus delivery of mitoxantrone for cancer therapy. Nanoscale 2018, 10, 16307–16313. [PubMed: 30129956]

(28). Franke CE; Czapar AE; Patel RB; Steinmetz NF Tobacco Mosaic Virus-Delivered Cisplatin Restores Efficacy in Platinum-Resistant Ovarian Cancer Cells. Mol. Pharmaceutics 2018, 15, 2922–2931.

(29). Poklar N; Pilch DS; Lippard SJ; Redding EA; Dunham SU; Breslauer KJ Influence of cisplatin intrastrand crosslinking on the conformation, thermal stability, and energetics of a 20-mer DNA duplex. Proc. Natl. Acad. Sci. U.S.A 1996, 93, 7606–7611. [PubMed: 8755522]

(30). Patel R; Czapar AE; Fiering S; Oleinick NL; Steinmetz NF Radiation Therapy Combined with Cowpea Mosaic Virus Nanoparticle in Situ Vaccination Initiates Immune-Mediated Tumor Regression. ACS Omega 2018, 3, 3702–3707. [PubMed: 29732445]

(31). Klug A The tobacco mosaic virus particle: structure and assembly. Philos. Trans. R. Soc., B 1999, 354, 531–535.

(32). Czapar AE; Steinmetz NF Plant viruses and bacteriophages for drug delivery in medicine and biotechnology. Curr. Opin. Chem. Biol 2017, 38, 108–116. [PubMed: 28426952]

(33). Jamieson ER; Lippard SJ Structure, Recognition, and Processing of Cisplatin-DNA Adducts. Chem. Rev 1999, 99, 2467–2498. [PubMed: 11749487]

(34). Makovec T Cisplatin and beyond: molecular mechanisms of action and drug resistance development in cancer chemotherapy. Radiol. Oncol 2019, 53, 148–158. [PubMed: 30956230]

(35). Sooriyaarachchi M; Narendran A; Gailer J Comparative hydrolysis and plasma protein binding of cis-platin and carboplatin in human plasma in vitro. Metallomics 2011, 3, 49–55. [PubMed: 21135941]

(36). Hegedüs L; van der Vijgh WJ; Klein I; Kerpel-Fronius S; Pinedo HM Chemical reactivity of cisplatin bound to human plasma proteins. Cancer Chemother. Pharmacol 1987, 20, 211–212. [PubMed: 2824080]

(37). Pettersen EF; Goddard TD; Huang CC; Couch GS; Greenblatt DM; Meng EC; Ferrin TE UCSF Chimera–a visualization system for exploratory research and analysis. J. Comput. Chem 2004, 25, 1605–1612. [PubMed: 15264254]

(38). Shirakura T; Kelson TJ; Ray A; Malyarenko AE; Kopelman R Hydrogel nanoparticles with thermally controlled drug release. ACS Macro Lett. 2014, 3, 602–606. [PubMed: 25419487]

(39). Tarannum M; Holtzman K; Dréau D; Mukherjee P; Vivero-Escoto JL Nanoparticle combination for precise stroma modulation and improved delivery for pancreatic cancer. J. Controlled Release 2022, 347, 425–434.

(40). Silk AW; Margolin K Cytokine therapy. Hematol. Oncol. Clin 2019, 33, 261–274.

(41). Vlad AM; Budiu RA; Lenzner DE; Wang Y; Thaller JA; Colonello K; Crowley-Nowick PA; Kelley JL; Price FV; Edwards RP A phase II trial of intraperitoneal interleukin-2 in patients with platinum-resistant or platinum-refractory ovarian cancer. Cancer Immunol. Immunother 2010, 59, 293–301. [PubMed: 19690855]

(42). Lizotte PH; Wen AM; Sheen MR; Fields J; Rojanasopondist P; Steinmetz NF; Fiering S In situ vaccination with cowpea mosaic virus nanoparticles suppresses metastatic cancer. Nat. Nanotechnol 2016, 11, 295–303. [PubMed: 26689376]

(43). Murray AA; Wang C; Fiering S; Steinmetz NF In situ vaccination with cowpea vs tobacco mosaic virus against melanoma. Mol. Pharmaceutics 2018, 15, 3700–3716.

(44). Shukla S; Roe AJ; Liu R; Veliz FA; Commandeur U; Wald DN; Steinmetz NF Affinity of plant viral nanoparticle potato virus X (PVX) towards malignant B cells enables cancer drug delivery. Biomater. Sci 2020, 8, 3935–3943. [PubMed: 32662788]

(45). Hu H; Steinmetz NF Doxorubicin-Loaded Physalis Mottle Virus Particles Function as a pH-Responsive Prodrug Enabling Cancer Therapy. Biotechnol. J 2020, 15, No. 2000077.

(46). Ramamurthi P; Zhao Z; Burke E; Steinmetz NF; Mullner M Tuning the Hydrophilic-Hydrophobic Balance of Molecular Polymer Bottlebrushes Enhances their Tumor Homing Properties. Adv. Healthcare Mater 2022, 11, No. e2200163.

(47). Bruckman MA; Randolph LN; VanMeter A; Hern S; Shoffstall AJ; Taurog RE; Steinmetz NF Biodistribution, pharmacokinetics, and blood compatibility of native and PEGylated tobacco mosaic virus nano-rods and-spheres in mice. Virology 2014, 449, 163–173. [PubMed: 24418549]

(48). Cataldi M; Vigliotti C; Mosca T; Cammarota M; Capone D Emerging role of the spleen in the pharmacokinetics of monoclonal antibodies, nanoparticles and exosomes. Int. J. Mol. Sci 2017, 18, 1249. [PubMed: 28604595]

(49). Mulvey JJ; Villa CH; McDevitt MR; Escorcia FE; Casey E; Scheinberg DA Self-assembly of carbon nanotubes and antibodies on tumours for targeted amplified delivery. Nat. Nanotechnol 2013, 8, 763–771. [PubMed: 24077028]

(50). Lee KL; Shukla S; Wu M; Ayat NR; El Sanadi CE; Wen AM; Edelbrock JF; Pokorski JK; Commandeur U; Dubyak GR; Steinmetz NF Stealth filaments: Polymer chain length and conformation affect the in vivo fate of PEGylated potato virus X. Acta Biomater. 2015, 19, 166–179. [PubMed: 25769228]

(51). Muro S; Garnacho C; Champion JA; Leferovich J; Gajewski C; Schuchman EH; Mitragotri S; Muzykantov VR Control of endothelial targeting and intracellular delivery of therapeutic enzymes by modulating the size and shape of ICAM-1-targeted carriers. Mol. Ther 2008, 16, 1450–1458. [PubMed: 18560419]

(52). Kolhar P; Anselmo AC; Gupta V; Pant K; Prabhakarpandian B; Ruoslahti E; Mitragotri S Using shape effects to target antibody-coated nanoparticles to lung and brain endothelium. Proc. Natl. Acad. Sci. U.S.A 2013, 110, 10753–10758. [PubMed: 23754411]

(53). Huang X-J; Choi Y-K; Im H-S; Yarimaga O; Yoon E; Kim H-S Aspartate aminotransferase (AST/GOT) and alanine aminotransferase (ALT/GPT) detection techniques. Sensors 2006, 6, 756–782.

(54). Sabbisetti VS; Ito K; Wang C; Yang L; Mefferd SC; Bonventre JV Novel assays for detection of urinary KIM-1 in mouse models of kidney injury. Toxicol. Sci 2013, 131, 13–25. [PubMed: 23019274]

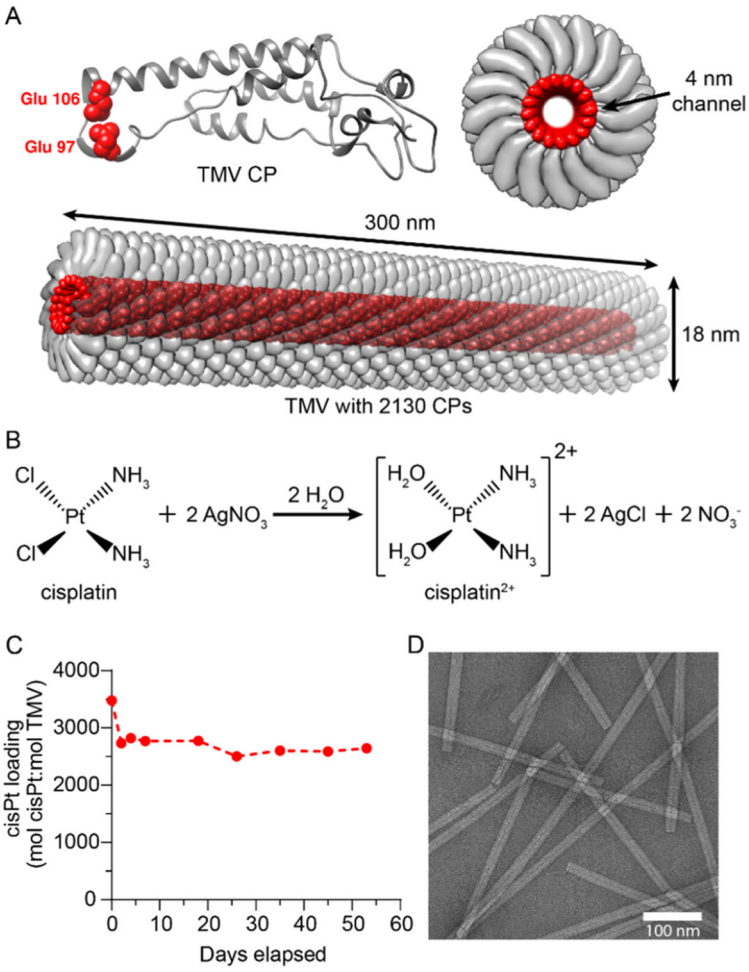

Figure 1.

Synthesis and characterization of TMV-cisPt. (A) Structures of TMV CP and TMV. TMV forms a 300 nm × 18 nm nanotube with a 4 nm wide channel. One TMV is composed of 2130 identical copies of a CP, and each CP has two glutamic acids labeled in red (Glu 97 and Glu 106) located inside of the 4 nm channel. The Glu side chains can interact with $cisPt^{2+}$ electrostatically to yield TMV-cisPt. All images were produced using the UCSF Chimera.[37] (B) Scheme of the reaction to produce $cisPt^{2+}$ using cisPt and $AgNO_3$. (C) $cisPt^{2+}$ loading was calculated using the molar ratio of cisPt concentration determined by ICP-MS and TMV concentration determined by UV–vis spectroscopy; TMV-cisPt was stable over 53 days. (D) TEM image of TMV-cisPt (negatively stained with uranyl formate) showed the typical high-aspect-ratio nanostructures comparable to that of native TMV.

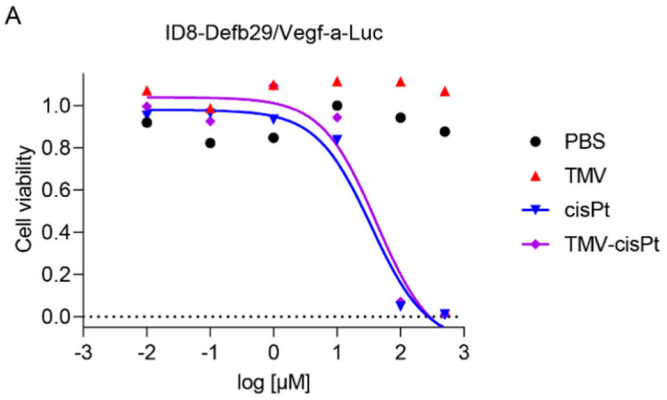

C

	IC_{50} (μM)	
Cell line	cisPt	TMV-cisPt
ID8-Defb29/Vegf-a-Luc	53.2	43.23
A2780	34.78	42.06

Figure 2.

Comparison of the cytotoxicity of cisPt and TMV-cisPt. (A) ID8-Defb29/Vegf-a-Luc and (B) A2780 cells were treated with cisPt and TMV-cisPt, using a concentration range of 0.01–500 μM. PBS and TMV were used as negative controls. Treatment lasted 24 h, then the MTT assay was performed. (C) IC_{50} values of cisPt and TMV-cisPt were calculated from the MTT assay results; TMV and PBS have no cytotoxic effects on the cells.

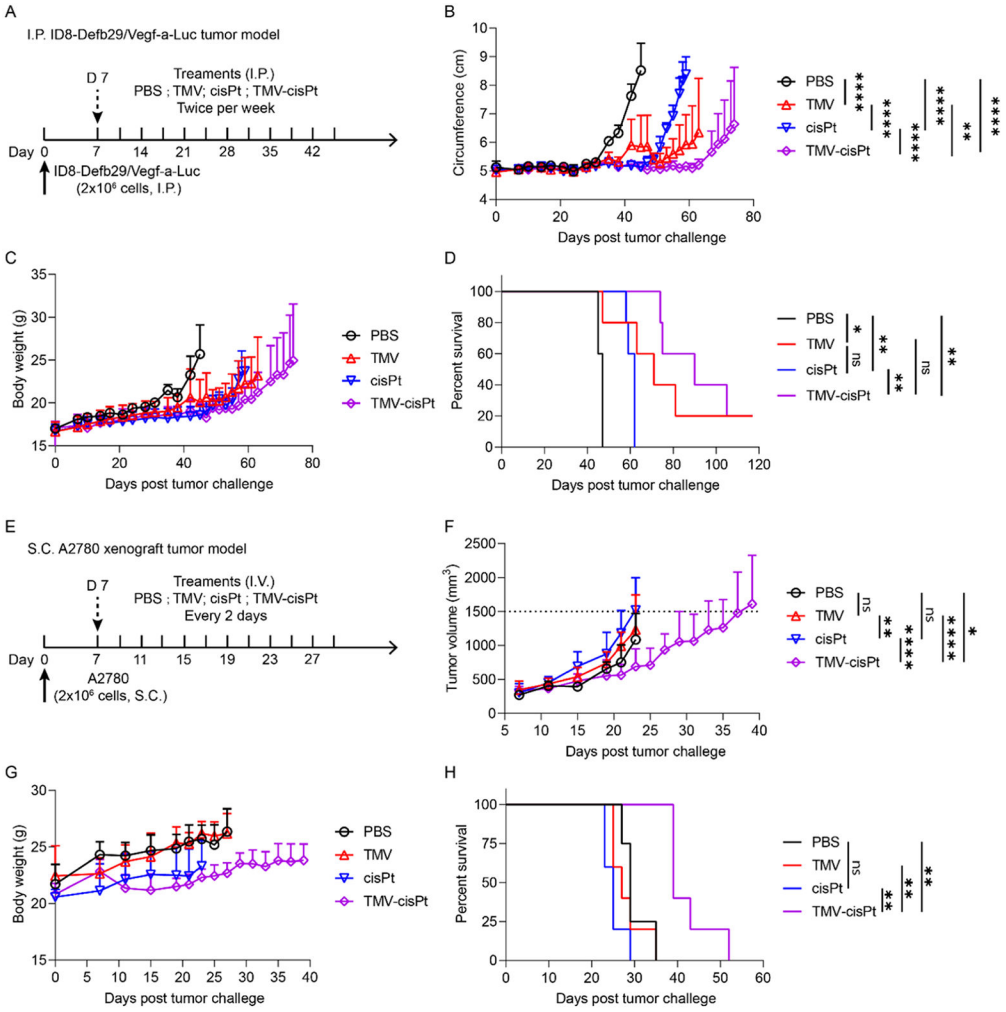

Figure 3.

Treatment of I.P. disseminated ID8-Defb29/Vegf-a-Luc ovarian tumors in C57BL/6 mice (A–D) and S.C. A2780 ovarian tumor xenografts in NCR nu/nu mice (E–H). (A) Experimental protocol for the ID8-Defb29/Vegf-a-Luc tumor study; 2×10^6 ID8-Defb29/Vegf-a-Luc cancer cells were I.P. injected into female C57BL/6 mice, $n = 5$. TMV-cisPt, cisPt, TMV, and PBS in 200 μL were administered I.P. twice per week starting 7 days post tumor inoculation for 6 weeks. The cisPt dose was 20 μg (which equates to ~1 mg TMV). Tumor progression was monitored by measuring the circumference (B), body weight (C), and overall survival (D). (E) Experimental protocol for S.C. A2780 tumor study; 2×10^6 A2780 cancer cells mixed with Matrigel were S.C. injected into the right flank of female NCR nu/nu mice, $n = 5$. TMV-cisPt, cisPt, TMV, and PBS in 100 μL were administered I.V. every 2 days starting 7 days post tumor inoculation until the tumor volume reached 1500 mm^3. The cisPt dose was 20 μg (which equates to 1 mg TMV). Tumor progression was monitored by measuring the tumor volume (F), body weight (G), and overall survival (H). Statistical analysis was performed using two-way ANOVA for (B) and (H) (with $^{**}p < 0.01$, $^{****}p < 0.0001$) and Log-Rank Mantel-Cox test for (D) and (H) (with $^{*}p < 0.05$, $^{**}p < 0.01$).

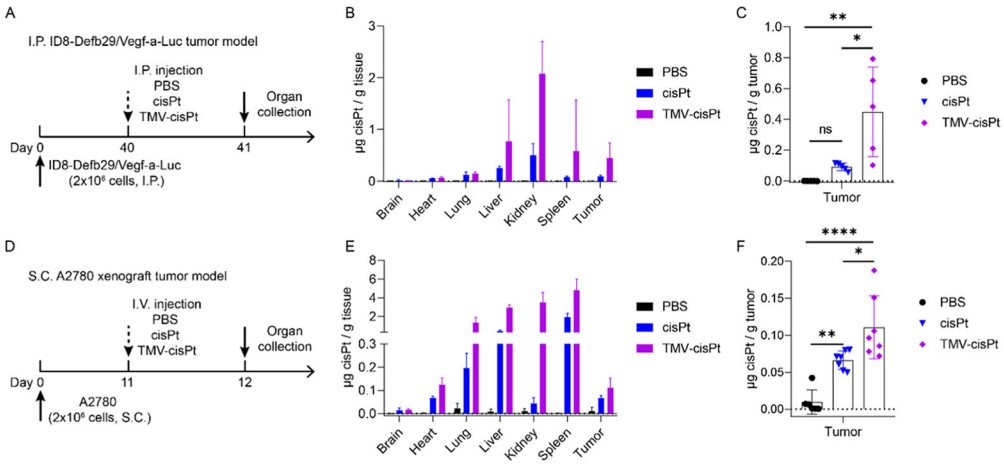

Figure 4.

Biodistribution of cisPt in organs and tumors comparing TMV-cisPt *vs* free cisPt. cisPt concentration was determined by ICP-MS 24 h after a single administration on day 40 for the I.P. ID8-Defb29/Vegf-a-Luc tumor model or on day 11 for the S.C. A2780 xenograft tumor model. (A, D) Experimental protocols. Biodistribution of cisPt in organs (B) and tumors (C) for the I.P. ID8-Defb29/Vegf-a-Luc tumor model ($n = 5$) and biodistribution of cisPt in organs (E) and tumors (F) for the S.C. A2780 tumor model ($n = 7$). Statistical analysis was performed using one-way ANOVA with Turkey's test for (C) and (F) (with *$p < 0.05$, **$p < 0.01$).

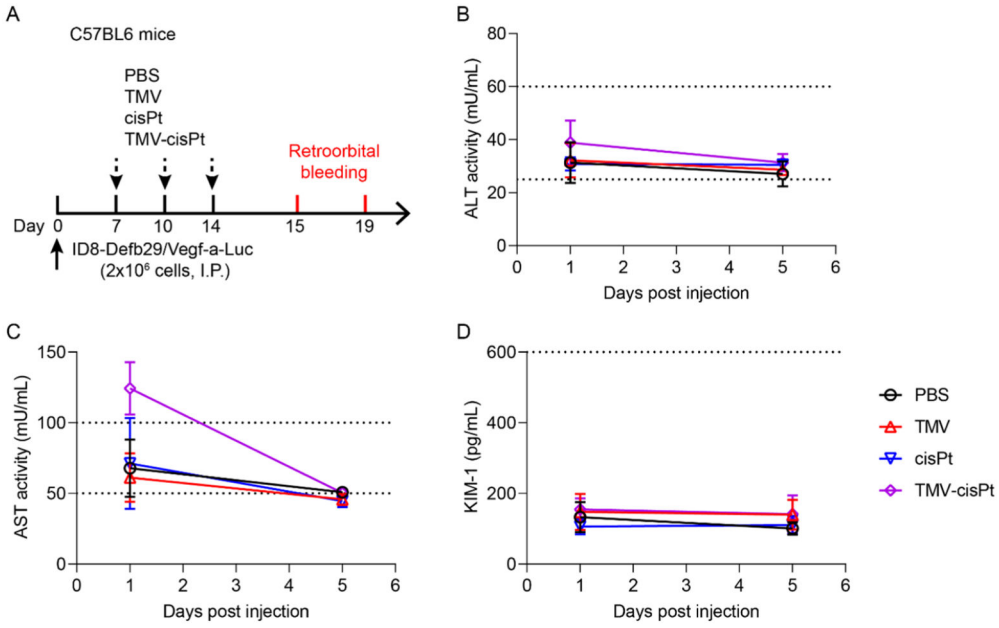

Figure 5.

Toxicity of TMV-cisPt, cisPt, and TMV in treated mice. (A) Experimental protocol. ALT (B), AST (C), and KIM-1 (D) levels on day 1 or day 5 post treatment (all animals received three doses of PBS, TMV, cisPt, and cisPt-TMV). Dashed lines indicate the normal ranges for ALT, AST, and KIM-1 in mice.